The Astrophysical Journal, 699:133–142, 2009 July 1 doi:10.1088/0004-637X/699/1/133

ENDPOINT BRIGHTENINGS IN ERUPTING FILAMENTS

Y.-M. Wang[1], K. Muglach[1,2], and B. Kliem[1,3,4]
[1] Space Science Division, Naval Research Laboratory, Washington, DC 20375-5352, USA; yi.wang@nrl.navy.mil, muglach@nrl.navy.mil
[2] ARTEP, Inc., Ellicott City, MD, USA
[3] MSSL, University College London, Holmbury St. Mary, Dorking, Surrey, UK
[4] Institut für Physik und Astronomie, Universität Potsdam, Potsdam, Germany; bkliem@uni-potsdam.de
Received 2009 February 28; accepted 2009 April 14; published 2009 June 10

ABSTRACT

Two well known phenomena associated with erupting filaments are the transient coronal holes that form on each side of the filament channel and the bright post-event arcade with its expanding double row of footpoints. Here we focus on a frequently overlooked signature of filament eruptions: the spike- or fan-shaped brightenings that appear to mark the far endpoints of the filament. From a sample of non-active-region filament events observed with the Extreme-Ultraviolet Imaging Telescope on the *Solar and Heliospheric Observatory*, we find that these brightenings usually occur near the outer edges of the transient holes, in contrast to the post-event arcades, which define their inner edges. The endpoints are often multiple and are rooted in and around strong network flux well outside the filament channel, a result that is consistent with the axial field of the filament being much stronger than the photospheric field inside the channel. The extreme ultraviolet brightenings, which are most intense at the time of maximum outward acceleration of the filament, can be used to determine unambiguously the direction of the axial field component from longitudinal magnetograms. Their location near the outer boundary of the transient holes suggests that we are observing the footprints of the current sheet formed at the leading edge of the erupting filament, as distinct from the vertical current sheet behind the filament which is the source of the post-event arcade.

Key words: Sun: corona – Sun: coronal mass ejections (CMEs) – Sun: filaments – Sun: magnetic fields – Sun: prominences – Sun: UV radiation

1. INTRODUCTION

Despite a continually growing body of observational and theoretical work, the physical nature of solar filaments/prominences remains poorly understood and controversial. Is the cool material supported against gravity within a collection of magnetic dips (Aulanier & Démoulin 1998; Chae et al. 2005; López Ariste et al. 2006), or does it form part of a dynamical system of chromospheric jets (Zirker et al. 1998; Litvinenko & Martin 1999; Wang 1999, 2001; Kucera et al. 2003; Lin et al. 2003, 2005)? Do filaments have the structure of a twisted flux rope (Low 1996; Aulanier et al. 1999; Gibson & Fan 2006a), or that of a sheared arcade which is transformed into a flux rope only as it begins to erupt (Antiochos et al. 1994; Martin & McAllister 1997)? Do they emerge from below the photosphere as fully fledged flux ropes (Rust & Kumar 1994; Titov & Démoulin 1999; Manchester et al. 2004; Lites 2005; Okamoto et al. 2008), or do they form by flux cancellation of surface fields (van Ballegooijen & Martens 1989; Zirker et al. 1997; Amari et al. 1999; Mackay et al. 2000; Yeates et al. 2007; Wang & Muglach 2007; Martin et al. 2008b; Yeates & Mackay 2009)? What is the role of magnetic reconnection (Antiochos et al. 1999; Moore et al. 2001; Amari et al. 2003; Sterling & Moore 2004, 2005), as opposed to ideal magnetohydrodynamic (MHD) instabilities (Roussev et al. 2003; Kliem et al. 2004; Fan 2005; Török & Kliem 2005), in triggering their eventual eruption?

In order to disentangle the magnetic structure of filaments, it is first necessary to determine the direction of the axial field component (for a review of this problem, see Martin et al. 2008a). In the context of line-of-sight magnetograph measurements, a 180° ambiguity may arise (as it does, for other reasons, in vector polarimetry: Metcalf et al. 2006) because it is often unclear where, and in particular on which side of the polarity inversion line (PIL), the endpoints of the filament lie. One approach is to assume that the direction of the filament field is the same as that in which chromospheric fibrils stream away from network flux concentrations, of known polarity, on either side of the filament channel (Foukal 1971). Another indirect approach is to employ an empirical rule involving the intermediate legs or "barbs" of the filament (Martin 1998; Pevtsov et al. 2003): if the barbs point forward and to the right (left), then the axial field points to the right (left) when viewed from the positive-polarity side of the PIL, and the filament has "dextral" ("sinistral") chirality. Alternatively, the direction of the axial field may be inferred from the skew (corresponding to right- or left-handed helicity) between the overlying coronal loops and the filament channel. The filaments in the northern (southern) hemisphere are found to be predominantly dextral (sinistral), with the overlying arcade having left-handed/negative (right-handed/positive) helicity. If the barbs are interpreted as concave-downward field lines, they are then rooted in minority-polarity flux on the "wrong" side of the PIL, and the filament itself has the opposite helicity to that of the overlying coronal loops (see Martin 2003). On the other hand, if the barbs trace out the concave-upward underside of a helical flux rope, or are associated with "bald patches" where the field lines just skim the solar surface (Aulanier & Démoulin 1998), the helicity of the filament matches that of the overlying arcade.

In many cases, information about the pre-eruption structure of a filament and the surrounding field can be gleaned from the behavior of the system after it erupts. If bright post-event loops are observed, their initial angle of skew relative to the PIL reveals the helicity of the overlying coronal arcade before the event. Another helicity indicator is the sense in which the filament rotates as it ascends (see Green et al. 2007; Rust & LaBonte 2005): in the case of a kink or other ideal MHD instability

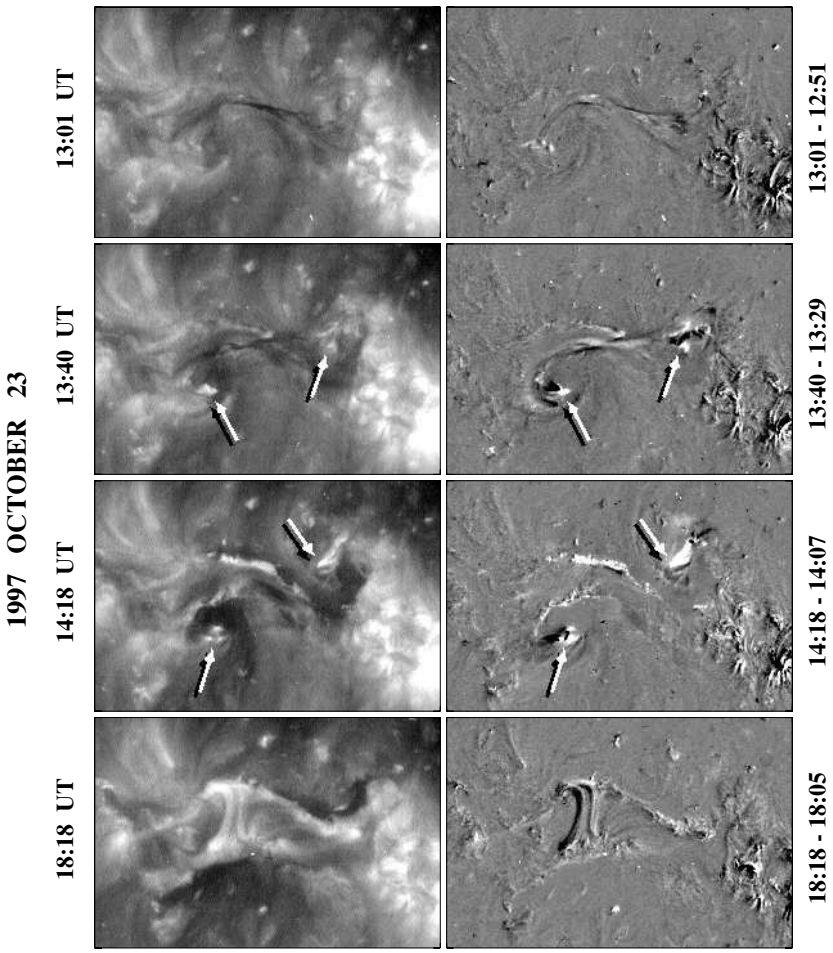

Figure 1. Eruption of a northern-hemisphere filament on 1997 October 23. Left panels: sequence of EIT Fe XII 19.5 nm images recorded at 13:01, 13:40, 14:18, and 18:18 UT. Right panels: corresponding running-difference frames, in which an observation taken ~12 minutes earlier is subtracted from the image at the left. Here and in subsequent figures, north is up and west is to the right; arrows point to EUV brightenings at the endpoints of the erupting filament.

where twist is converted into writhe, the rotation is expected to be clockwise (counterclockwise) as viewed from above, if the net helicity of the erupting system is right handed (left handed).

This investigation is concerned with an often-overlooked signature of filament eruptions: the bright features that mark the far extremities of the filaments, thereby allowing a straightforward determination of the axial field direction. In the next section, we describe examples of such endpoint brightenings observed in the extreme ultraviolet (EUV) during 1997–2005, and identify the corresponding locations on longitudinal magnetograms of the photospheric field. In Section 3, we address the question of the physical origin of these brightenings. Our conclusions are summarized in Section 4.

2. OBSERVATIONAL CASE STUDIES

The Extreme-Ultraviolet Imaging Telescope (EIT) on the *Solar and Heliospheric Observatory* (*SOHO*) records full-disk images with a 2-pixel resolution of 5″ in each of the four emission lines Fe IX/X 17.1 nm, Fe XII 19.5 nm, Fe XV 28.4 nm, and He II 30.4 nm (Delaboudinière et al. 1995). In the routine synoptic mode, images are taken every ~12 minutes in Fe XII 19.5 nm (with maximum temperature response at ~1.4 MK), but only once every 6 hr in the other bandpasses. From the large database accumulated since 1996, we have chosen nine events that provide especially clear illustrations of endpoint brightenings during the eruption of "quiescent" (non-active-region) filaments.

In order to relate the EUV features to the underlying photospheric field, we employ line-of-sight magnetograms recorded in the Ni I 676.8 nm line with the Michelson Doppler Imager (MDI; Scherrer et al. 1995) on *SOHO*. Full-disk, synoptic-mode images having a 2-pixel resolution of 4″ are taken at 96-minute intervals throughout the day, beginning at approximately 00:00 UT.[5] Most of these magnetograms are 1-minute observations with a noise level of ~30 G; the rest are 5-minute averages with a noise level of ~15 G. In addition, continuous 1-minute cadence data are taken during MDI campaigns. When such campaign-mode magnetograms were available during the filament event, we constructed our own 5-minute averages from them; otherwise, we employed the synoptic magnetogram recorded closest in time to the given 19.5 nm observation. After correcting for the factor of 1.31 difference in the plate scales, we co-aligned the EIT and MDI images using the center of the solar disk as the common reference point. The co-alignment was checked by blinking between EUV bright points and the corresponding small magnetic bipoles.

2.1. 1997 October 23

The left-hand panels of Figure 1 show the eruption of a quiescent filament in the northern hemisphere during 1997 October 23, as observed in Fe XII 19.5 nm. In order to bring

[5] See http://soi.stanford.edu.

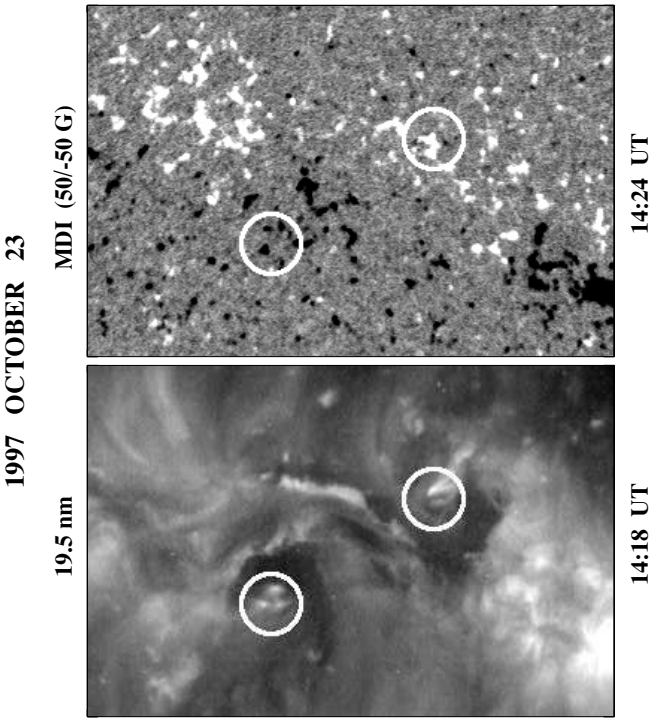

Figure 2. Photospheric flux distribution underlying the filament eruption of 1997 October 23. Top: MDI synoptic magnetogram (5-minute average) recorded at 14:24 UT. Gray-scale levels for the line-of-sight field range between $B_{los} < -50$ G (black) and $B_{los} > +50$ G (white). Bottom: Fe XII 19.5 nm image taken at 14:18 UT. The locations of the endpoint brightenings are circled in both the MDI and the EIT image.

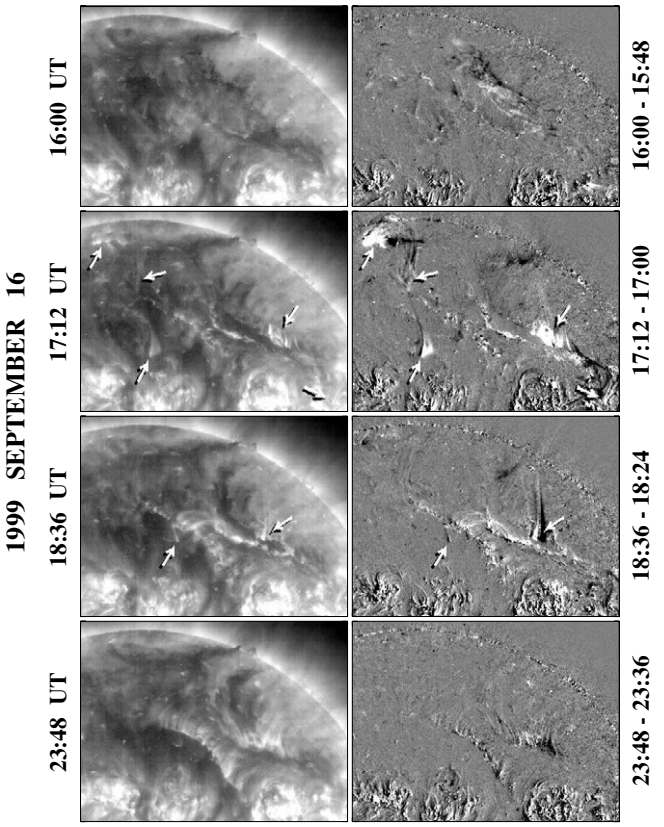

Figure 3. Eruption of a northern-hemisphere filament on 1999 September 16. Left panels: sequence of Fe XII 19.5 nm images recorded at 16:00, 17:12, 18:36, and 23:48 UT. Right panels: corresponding running-difference frames. Multiple endpoint brightenings (marked by arrows) are observed over a wide area.

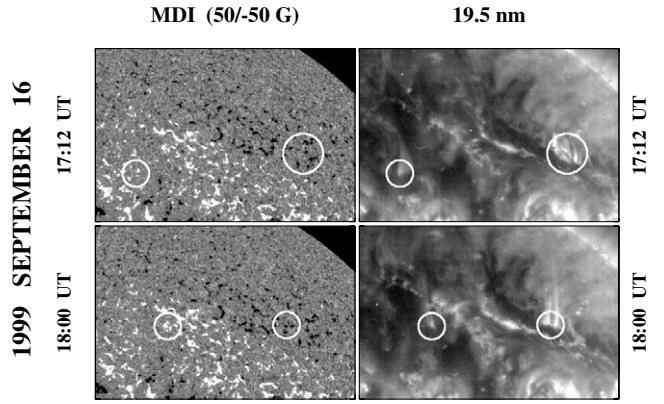

Figure 4. Photospheric flux distribution underlying the filament eruption of 1999 September 16. Left panels: MDI line-of-sight magnetograms recorded at 17:12 and 18:00 UT (5-minute averages constructed from higher cadence data). Gray scale is again saturated at $B_{los} = \pm 50$ G. Right panels: simultaneous Fe XII 19.5 nm images. The locations of the main endpoint brightenings are circled in both the MDI and EIT images.

out changes in the brightness and/or position of the features, the right-hand panels display the difference between the image on the left and one recorded ∼12 minutes earlier. As the filament rises, its axis rotates counterclockwise by ∼45°. A post-event arcade forms after ∼13:29 UT, with its double row of footpoints centered on the curved filament channel and spreading outward from it; the initial angle of skew of the reconnected loops indicates left-handed helicity. The arrows point to the EUV enhancements at the endpoints of the erupting filament. These brightenings are situated near the outer edges of the transient holes (or "dimming regions") that form on the southeast and northwest sides of the post-event arcade. The ends of the filament in fact consist of multiple dark threads that splay out from the filament axis or spine, with the brightenings concentrated near their bases.

Comparing the EIT image recorded at 14:18 UT with a co-aligned MDI magnetogram taken at 14:24 UT (Figure 2), we see that the endpoint brightenings are located in strong unipolar network flux well away from the PIL. Since the northwest (southeast) end of the filament is rooted in positive- (negative-) polarity flux, the axial field component points to the right when viewed from the positive-polarity region, so the filament is dextral. In agreement with the empirical rule of Martin (1998), an Hα image taken at the Big Bear Solar Observatory (BBSO) on October 22 shows that the pre-eruption filament has right-bearing barbs.[6] The counterclockwise rotation observed during the eruption suggests that the filament and its magnetic environment have net left-handed helicity.

In association with this filament event, the Large Angle and Spectrometric Coronagraph (LASCO; Brueckner et al. 1995) on *SOHO* observed a halo coronal mass ejection (CME) which entered the ∼2–6 $R_\odot$ LASCO C2 field of view at ∼12:42 UT.[7] This wide, predominantly northern-hemisphere CME had an average sky-plane speed of ∼500 km s^{-1}. No Hα flare was recorded in the National Geophysical Data Center (NGDC) archive for this or any of our other events.

[6] See http://bbso.njit.edu

[7] See http://cdaw.gsfc.nasa.gov/CME_list

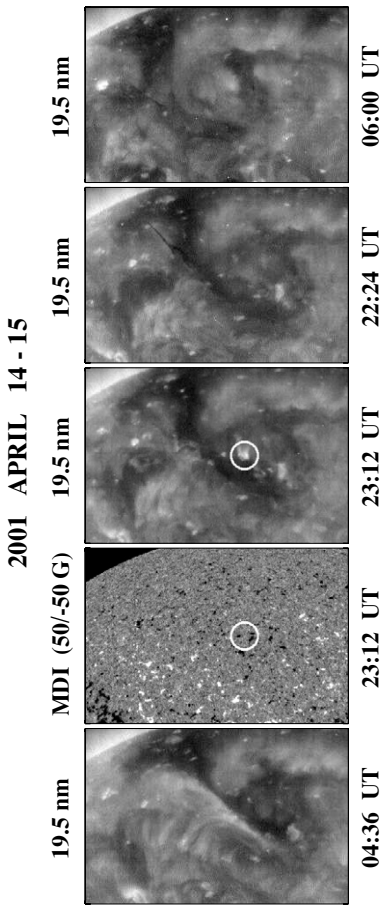

Figure 5. Eruption of a northern-hemisphere filament during 2001 April 14–15. Top three panels: Fe XII 19.5 nm images recorded at 06:00, 22:24, and 23:12 UT, respectively. Fourth panel: MDI line-of-sight magnetogram taken around 23:12 UT (5-minute average of higher cadence data). Bottom panel: 19.5 nm image recorded at 04:36 UT on April 15. The location of the endpoint brightening is circled in the EIT image and magnetogram taken at 23:12 UT.

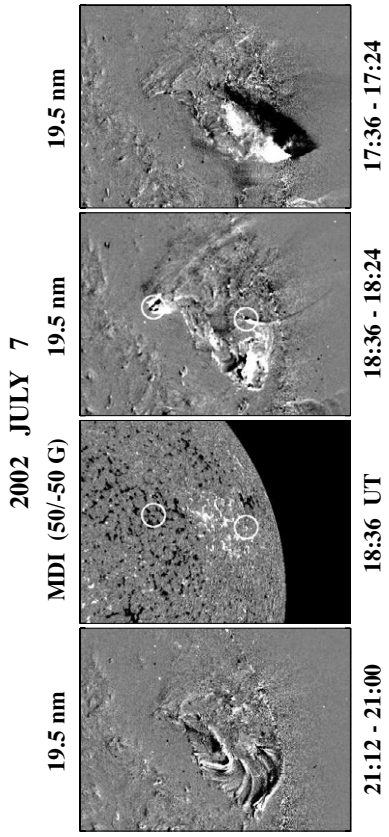

Figure 6. Eruption of a filament on 2002 July 7. Top panel: Fe XII 19.5 nm running-difference image taken at 17:36 UT. Second panel: 19.5 nm running-difference image taken at 18:36 UT. Third panel: MDI line-of-sight magnetogram centered at 18:36 UT (5-minute average of higher cadence data). Bottom panel: 19.5 nm running-difference image taken at 21:12 UT. The locations of the endpoint brightenings are circled in the EIT image and magnetogram recorded at 18:36 UT.

2.2. 1999 September 16

Figure 3 shows the eruption of a large northern-hemisphere filament on 1999 September 16. In this case, multiple endpoint brightenings are observed over a wide area as the filament accelerates outward; the eruption also appears to destabilize a branch of the filament system that connects to the northeast polar region and one that extends to the periphery of the active region near the west limb. Again, the spike- or sheet-like EUV enhancements are located in strong unipolar network well outside the PIL and the initial post-event arcade system (Figure 4). Since the southern end of the erupting filament is anchored in the negative-polarity region to the west of the main filament channel, it is evident that the axial field points to the right as viewed from the positive-polarity region, an inference that is further supported by the presence of right-bearing barbs in BBSO Hα images taken during the preceding days. The slant of the post-eruption loops in the 19.5 nm image recorded at 18:36 UT (Figure 3) indicates that the overlying arcade has left-handed helicity.

In association with this event, a white-light CME containing thread-like fine structure was observed above the north pole. The CME entered the LASCO C2 field of view after 17:00 UT and accelerated to speeds in excess of $\sim$1000 km s^{-1}.

2.3. 2001 April 14

In Figure 5, a filament near the boundary of the north polar hole is seen rising slowly and then erupting after $\sim$22:24 UT. Subsequently, a fan-shaped EUV brightening appears along the northern edge of the dark transient hole to the west of the filament channel. As shown in the MDI magnetogram (fourth panel of Figure 5), the brightening occurs in the vicinity of strong negative-polarity network elements far from the PIL. The filament is dextral, with the axial field pointing southwestward; the skew of the post-eruption loops indicates left-handed helicity. BBSO Hα images recorded on April 13 show right-bearing barbs.

A gradually accelerating CME, consisting of a diffuse partial halo with a narrow, relatively bright ejection on its northeast flank, emerged into the LASCO C2 field of view after 23:54 UT.

2.4. 2002 July 7

In Figure 6, a sheet-like filament is seen erupting near the west limb on 2002 July 7. Spiky EUV features are observed at the east end of the large post-event arcade and on its northwest side. The bright eastern anchor point lies within strong negative-polarity network flux (see Figure 6, third panel) near the boundary of a long equatorward extension of the north polar hole. The axial field points eastward and the filament is dextral, in accord with the right-bearing barbs visible in BBSO Hα images during the preceding days.

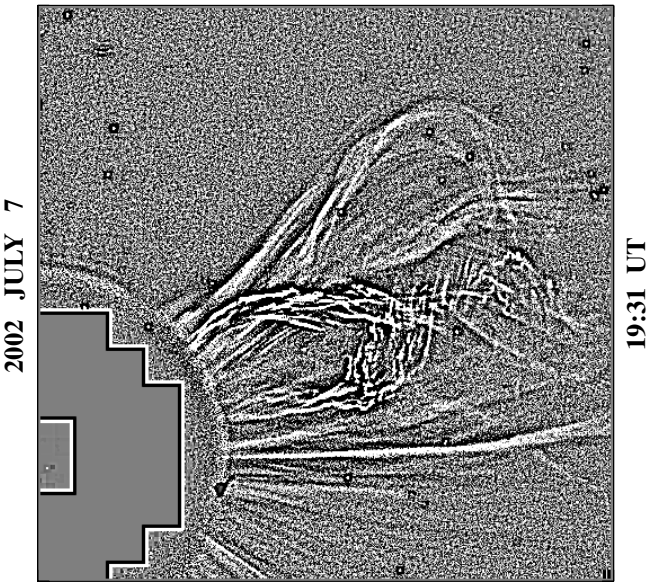

Figure 7. Edge-enhanced LASCO C2 image showing the white-light CME associated with the filament eruption of 2002 July 7. The occulting disk extends out to heliocentric radius $r \sim 2\ R_{\odot}$. The slant of the fine threads suggests that the ejected flux rope has left-handed helicity.

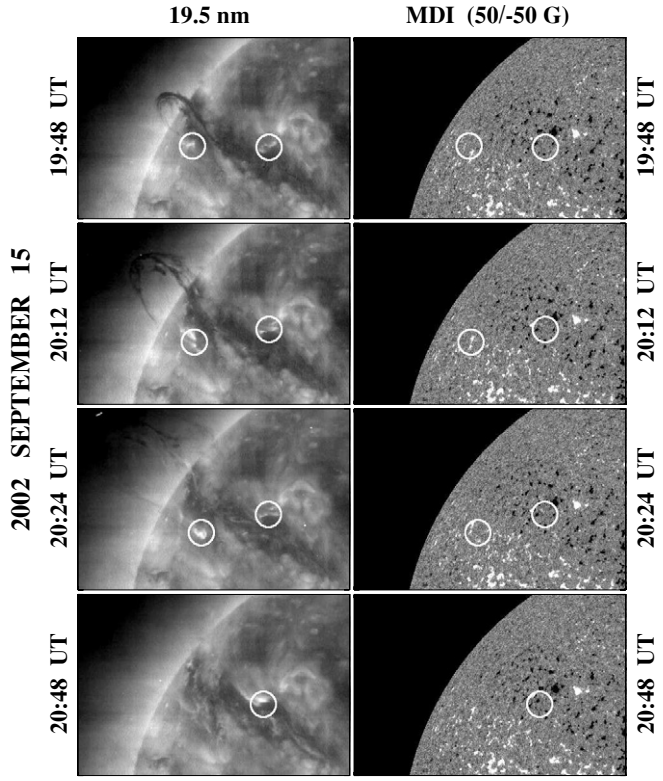

Figure 8. Eruption of a filament near the northeast limb on 2002 September 15. Left panels: sequence of Fe XII 19.5 nm images recorded at 19:48, 20:12, 20:24, and 20:48 UT. Right panels: corresponding MDI line-of-sight magnetograms (5-minute averages of higher cadence data). The locations of the endpoint brightenings are circled.

The CME that emerged into the LASCO C2 field of view at ~18:30 UT had an average speed of ~750 km s^{-1}. It contained a bright flux rope with many fine, parallel threads (Figure 7); if the upward-slanting threads are taken to be in the foreground, the structure has left-handed helicity.

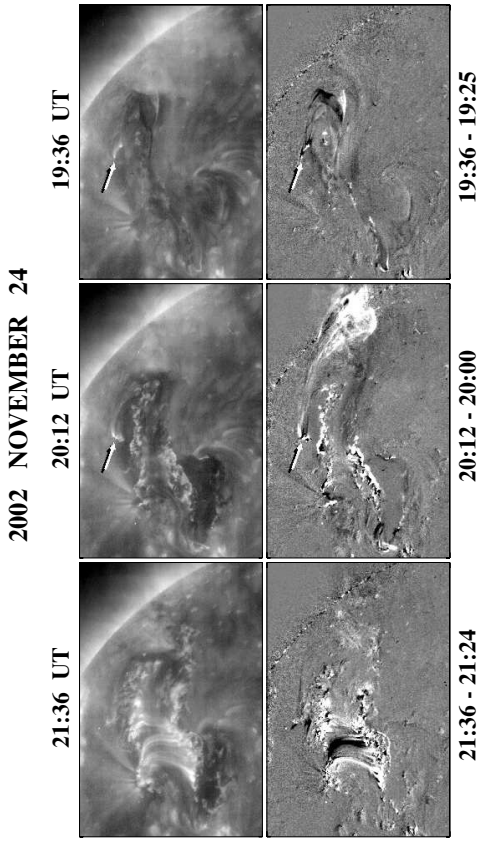

Figure 9. Eruption of a filament on 2002 November 24. Left panels: sequence of Fe XII 19.5 nm images recorded at 19:36, 20:12, and 21:36 UT. Right panels: corresponding running-difference frames.

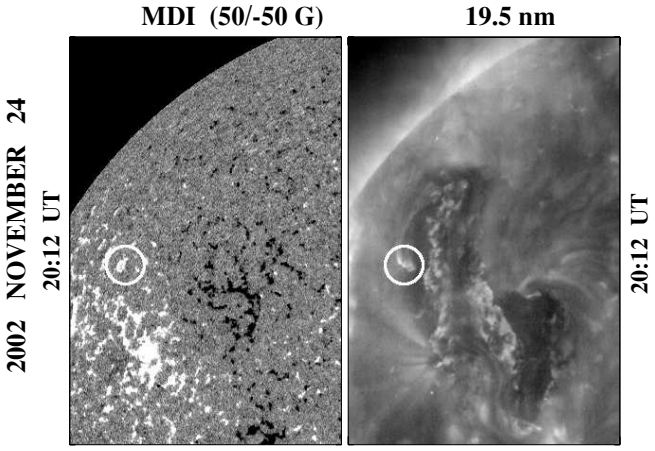

Figure 10. Photospheric flux distribution underlying the filament eruption of 2002 November 24. Left: MDI line-of-sight magnetogram recorded around 20:12 UT (5-minute average of higher cadence data). Right: Fe XII 19.5 nm image taken at 20:12 UT.

2.5. 2002 September 15

In this event near the northeast limb on 2002 September 15 (Figure 8), the filament undergoes a counterclockwise rotation as it rises. Spike-like EUV brightenings are observed to the east and west of the filament channel, where the long, dark strands of the erupting filament are anchored. The locus of the limbward brightenings swings southwestward as the filament rotates; as in the example of 1997 October 23, these apparent footpoint motions are due to the successive lighting-up of the

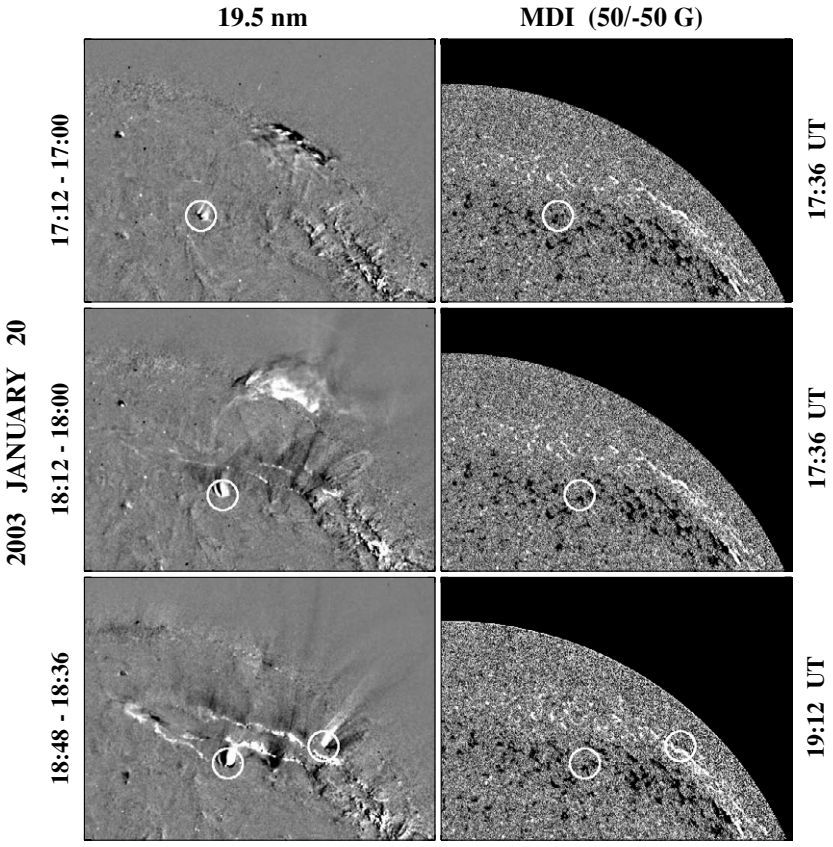

Figure 11. Eruption of a high-latitude filament on 2003 January 20. Left panels: Fe XII 19.5 nm running-difference images taken at 17:12, 18:12, and 18:48 UT, respectively. Right panels: corresponding MDI synoptic magnetograms (1-minute data).

multiple, splayed-out threads of the filament. As indicated by the magnetograms in Figure 8, the filament is dextral, with its axial field pointing to the right (westward) as viewed from the positive-polarity region. BBSO Hα images show right-bearing barbs.

A cone-shaped CME with an average speed of $\sim$770 km s^{-1} entered the LASCO C2 field of view at $\sim$21:30 UT.

2.6. 2002 November 24

Figure 9 shows the eruption of a north–south-oriented filament near the northeast limb on 2002 November 24. In this event, spike-like brightenings are clearly visible only on the eastern side of the filament channel, where the northern end of the filament appears to be anchored. From the 19.5 nm images taken after 20:00 UT, it is evident that these brightenings are located at the outer edge of the large transient hole that forms during that time, and that they initially lie well outside the footpoints of the post-event arcade. From the magnetogram in Figure 10, we conclude that the filament is dextral. An Hα image recorded by the Kanzelhöhe Solar Observatory at 10:02 UT shows clearly the presence of right-bearing barbs. From the apparent counterclockwise rotation of the post-eruption loops as they spread to cover the large transient holes, we deduce that the overlying arcade has left-handed helicity.

A very wide, quasi-halo CME with a speed in excess of 1000 km s^{-1} was observed over the northern hemisphere after $\sim$20:30 UT. This major white-light event was preceded by a gradual outward-stretching of the helmet streamer overlying the filament (the global magnetic configuration is illustrated in Figure 15(d) below).

2.7. 2003 January 20

In this event near the northwest limb (Figure 11), endpoint brightenings are first observed on the southeast side of the filament channel. As the filament rises, these features migrate southwestward along a path that coincides approximately with the outer edge of the (subsequently forming) transient hole. The brightenings increase in intensity as the filament accelerates outward and the transient holes appear. At 18:48 UT, a spike-like feature is also seen on the limbward side of the filament channel. After the filament is ejected, the outer edges of the transient holes brighten along their entire length, forming lines that run roughly parallel to the double row of post-event arcade footpoints. From the magnetograms in Figure 11, we see that the eastern end of the erupting structure is anchored inside a negative unipolar region, so that the filament is dextral. As predicted by the barb–chirality relationship of Martin, BBSO Hα images taken during the preceding days show right-bearing barbs. The post-eruption loops appear to rotate counterclockwise, consistent with left-handed helicity.

The event produced a classical bulb-shaped CME with bright leading edge, cavity, and core containing the twisted filament. The CME emerged into the LASCO C2 field of view after 18:30 UT and had a velocity of order 700 km s^{-1}.

2.8. 2003 September 24

In the southern-hemisphere example displayed in Figure 12, strong and relatively concentrated brightenings occur at the northwest end of the filament, while weaker and more dispersed EUV enhancements are seen along the multiple, curved threads at its southeast end. That the dark filament extends so far

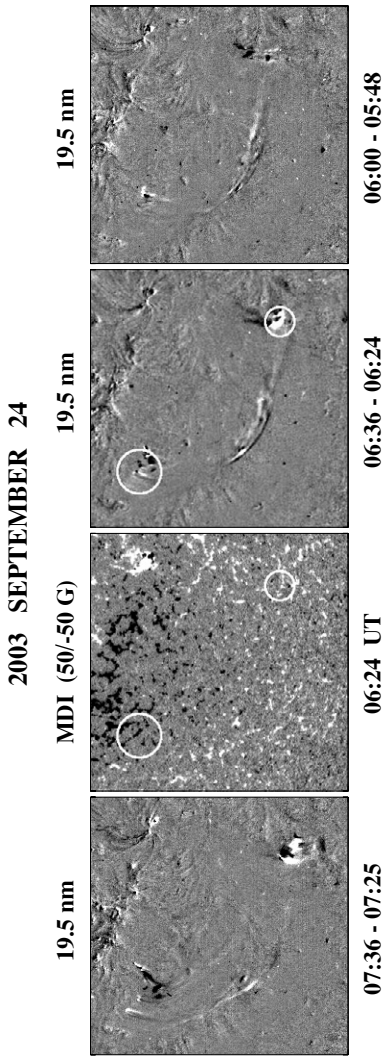

Figure 12. Eruption of a southern-hemisphere filament on 2003 September 24. Top panel: Fe XII 19.5 nm running-difference image taken at 06:00 UT. Second panel: 19.5 nm running-difference image taken at 06:36 UT. Third panel: MDI synoptic magnetogram recorded at 06:24 UT (5-minute average). Bottom panel: 19.5 nm running-difference image taken at 07:36 UT. The locations of the endpoint brightenings are circled in the middle two panels.

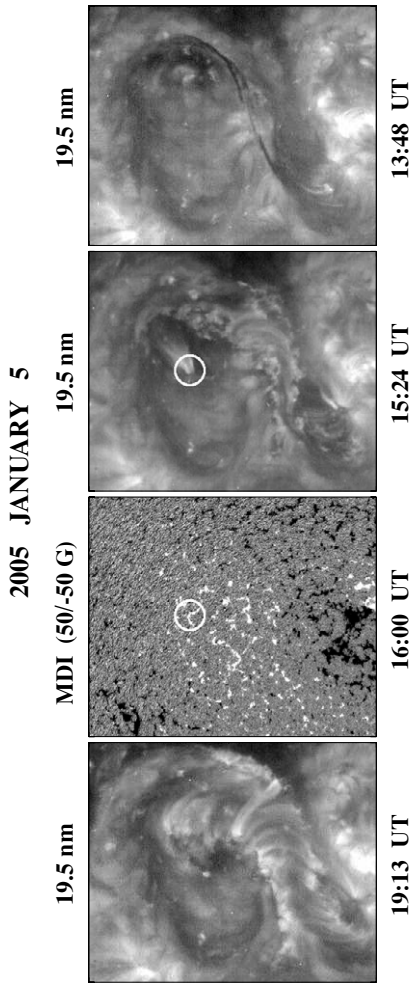

Figure 13. Eruption of a northern-hemisphere filament on 2005 January 5. Top panel: Fe XII 19.5 nm image taken at 13:48 UT. Second panel: 19.5 nm image taken at 15:24 UT. Third panel: MDI synoptic magnetogram recorded at 16:00 UT (1-minute data). Bottom panel: 19.5 nm image taken at 19:13 UT. The location of the fan-shaped brightening is circled in the two middle panels.

northward only becomes clear as it lifts off. As indicated by the magnetogram, the filament is sinistral, with the axial field pointing southeastward. BBSO Hα images recorded during the preceding days show left-bearing barbs.

A faint, blob-like ejection, presumably associated with this event, appeared in the southwest quadrant of the LASCO C2 field of view after ~09:00 UT.

2.9. 2005 January 5

The top panel of Figure 13 shows a northern-hemisphere filament with a reverse-S shape, as in the example of Figure 1. In the 19.5 nm image at 15:24 UT, taken just after the eruption (which occurs during an EIT data gap), a large fan-shaped structure appears at the outer edge of the transient hole that has formed within the upper crook of the reverse-S. From the magnetogram, we see that this endpoint brightening is located inside a positive unipolar region, so that the filament is dextral, as is consistent with the presence of right-bearing barbs in EIT He II 30.4 nm images recorded before the event. The post-eruption loops undergo an apparent counterclockwise rotation, indicating left-handed helicity, which in turn is in accordance with the reverse-S shape of the filament.

The event gave rise to a halo-like CME containing stringy filament material headed toward the southeast. The ejection emerged into the LASCO C2 field of view at 15:30 UT, with a speed in excess of 700 km s^{-1}.

3. PHYSICAL INTERPRETATION

From the examples of the last section, we conclude that there are in general two distinct kinds of footpoint brightenings associated with the eruption of non-active-region filaments: (1) the well known "double-ribbon" brightenings underlying the post-event loop arcade; and (2) spike-like brightenings occurring at the far endpoints of the erupting filament and located well outside the filament channel itself. The progressively expanding double-ribbon brightenings define the inner edges of the transient coronal holes, whereas the endpoint brightenings usually lie near or at their outer edges.

Transient coronal holes are the footpoint areas of coronal loops that have been forced open or stretched outward to great heights during a CME event (Kahler & Hudson 2001; de Toma et al. 2005; Attrill et al. 2006; McIntosh et al. 2007; Reinard & Biesecker 2008). It is generally accepted that the

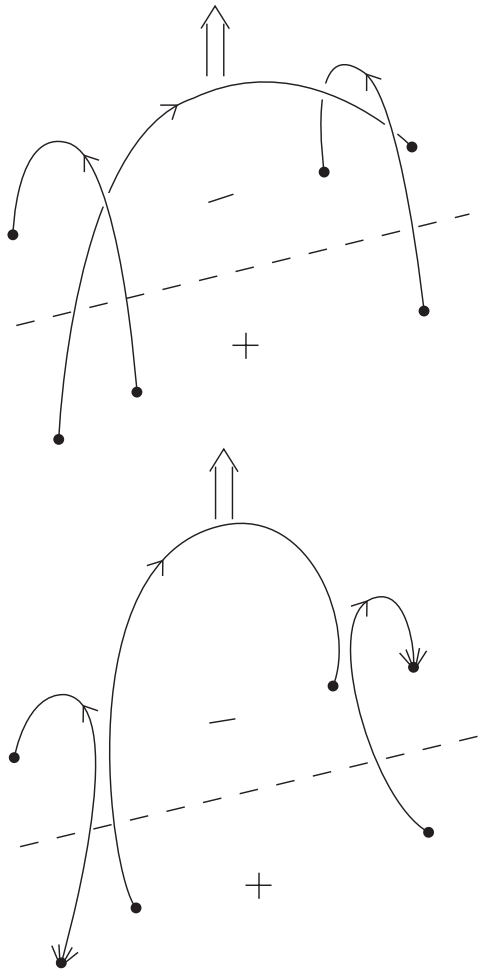

Figure 14. Endpoint brightenings produced by field-line reconnection between a rising filament and the overlying coronal loops. Although enhanced heating due to precipitating electrons occurs at all footpoints, the brightenings are concentrated at the original endpoints of the filament rather than at the footpoints of the background loops, which undergo a smaller change in temperature and are dispersed over a wider area.

post-event arcade forms as successive pairs of opposite-polarity open field lines come together and reconnect at an X-point or vertical current sheet located below the ejected filament (Kopp & Pneuman 1976; Moore et al. 2001). The double row of footpoint brightenings thus marks the inner boundary of the transient holes as they progressively fill in. In contrast, most of the endpoint brightenings are localized near the outer boundary between the transient holes and the surrounding closed-field regions. It is thus natural to attribute them to reconnection occurring at the interface between the erupting filament and the background corona, where strong currents are generated due to the compression and rapid change in the direction of the field (see, e.g., the simulation of Kliem et al. 2004, where a helical current sheet forms at the boundary between a kink-unstable flux rope and the surrounding medium). The spike-like brightenings presumably result from chromospheric evaporation in response to the downward flux of energetic electrons from the reconnection sites.

The cartoon in Figure 14 illustrates one scenario for the production of endpoint brightenings. As a leg of the filament is suddenly pulled upward into a vertical orientation, one of its strands runs into an overlying background loop that spans the filament channel. Reconnection then leads to an exchange of footpoints, such that the endpoint of the filament becomes connected to the far end of the coronal loop, and the near end of the loop becomes the new endpoint of the filament. Such footpoint exchanges are seen in three-dimensional MHD simulations in which twisted flux ropes undergo a loss of equilibrium and then reconnect with the overlying coronal arcade as they expand upward (Amari et al. 2003; Roussev et al. 2003; Török & Kliem 2005; Gibson & Fan 2006b, 2008; compare our Figure 14 with Figure 4(a) in Gibson & Fan 2006b).

An alternative scenario would be that the endpoint brightenings have their origin in the vertical current sheet below the filament, but are associated with the upward reconnection outflow rather than with the collapsing post-eruption loops. However, unless the pinch-off occurs very close to the filament spine, the footpoints of the reconnected flux-rope field lines would be significantly displaced from the axis endpoints, where the EUV enhancements are observed.

That the filament endpoints lie in strong unipolar network far from the PIL can be understood from magnetic flux conservation. Only in such regions is there sufficient photospheric flux to anchor the axial field of the filament. By the same token, the observed splaying-out of the endpoint threads may indicate that the axial field built up during the lifetime of the filament is so strong that it cannot be rooted in a single flux concentration. The tendency for the filament to hook backward as it leaves the filament channel, forming an S or reverse-S structure, may be dictated by the requirement that the field approach a more potential configuration in this region.

In most of the events displayed in Section 2, multiple endpoint brightenings are seen, ranged along the outer boundaries of the transient holes. The endpoints located closest to the filament channel (as measured along the axis of the filament) light up before the more distant ones, so that the locus of brightenings sometimes appears to rotate. The rotation is in the counterclockwise sense for reverse-S filaments in the northern hemisphere.

The observation of dark threads rooted in strong unipolar network far from the PIL seems to conflict with the classical picture of filaments as collections of magnetic dips. Since the component of the field normal to the photosphere would be expected to dominate near the endpoints, cool material could not be supported statically against gravity in such regions. This problem does not arise if the filament represents a dynamical system of counterstreaming flows, perhaps driven and maintained by reconnnection events in the chromosphere (Zirker et al. 1998; Litvinenko & Martin 1999; Wang 1999, 2001; Kucera et al. 2003; Lin et al. 2003, 2005).

In order to place the events of Section 2 in the context of the global coronal field, we have applied a potential-field source-surface (PFSS) extrapolation to the corresponding Carrington maps of the photospheric field from the National Solar Observatory (NSO/Kitt Peak). Figure 15 illustrates the results for four of our cases. Altogether, we find that five of the nine filament events (those of 1999 September 16, 2001 April 14, 2002 July 7, 2002 September 15, and 2005 January 5) occurred underneath "pseudostreamers," which separate coronal holes of the same polarity, while the rest were associated with helmet streamers separating holes of opposite polarity. Because the X-point where the open and closed field domains intersect is located at relatively low heights in pseudostreamers, this configuration may tend to facilitate the escape of filaments (cf. Liu & Hayashi 2006). On the other hand, the filament eruption of 2002 November 24 took place under a helmet streamer and gave rise to a

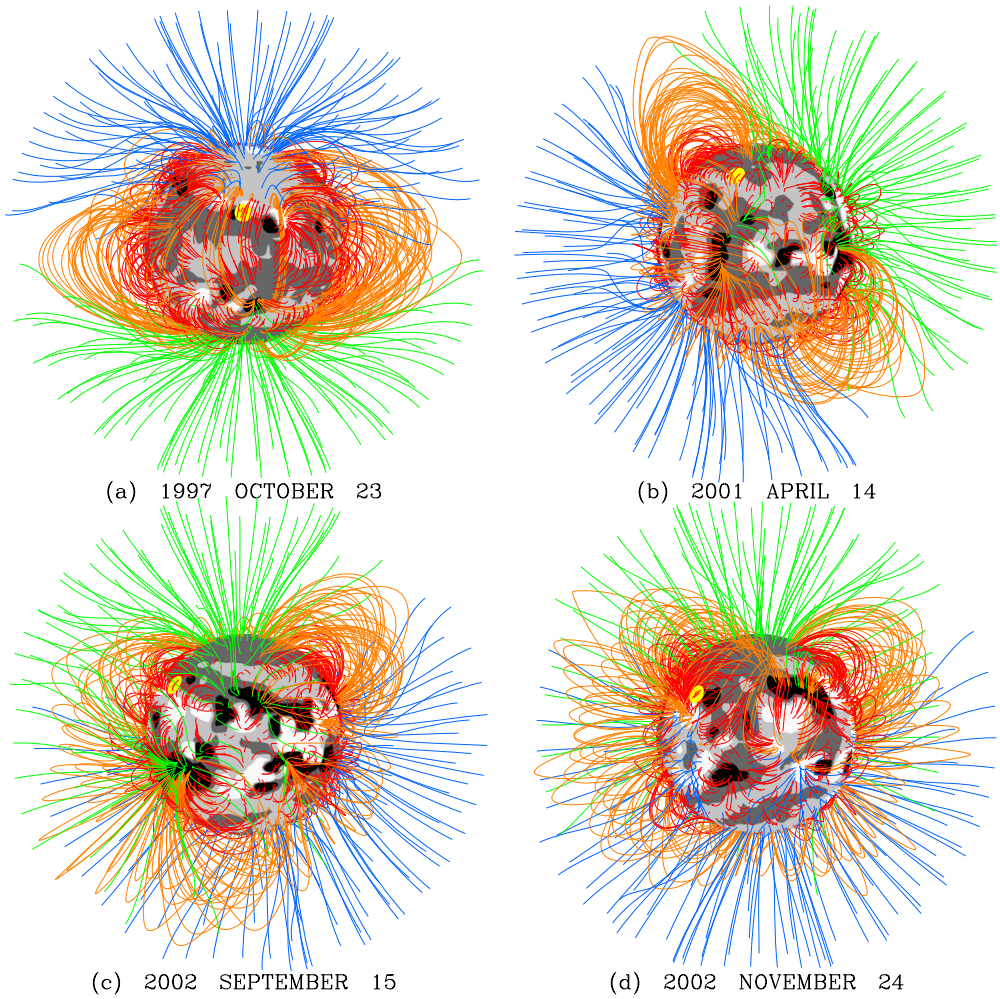

Figure 15. Global field-line configuration for four of the events described in Section 2: (a) 1997 October 23, (b) 2001 April 14, (c) 2002 September 15, and (d) 2002 November 24. Here, a PFSS extrapolation with source surface at $r = 2.5\ R_\odot$ was applied to NSO/Kitt Peak maps of the photospheric field. Closed loops are coded orange if they extend beyond $r = 1.5\ R_\odot$, red otherwise; open field lines are blue (green) if they have positive (negative) polarity. Black, dark gray, light gray, and white denote areas of the photosphere where the radial field component lies in the ranges $B_r < -10$ G, -10 G $< B_r < 0$ G, 0 G $< B_r < +10$ G, and $B_r > +10$ G, respectively. Yellow dot marks the approximate location of the filament eruption.

large, fast CME. In this case, as may be seen from Figure 15(d), the background field had a simple dipole-like configuration, suggesting that a multipolar geometry is not a necessary precondition for an eruption.

4. CONCLUSIONS

We have presented many examples of EUV brightenings that occur at the far endpoints of erupting quiescent filaments. These spike-like features, observed in Fe XII 19.5 nm (and, when images are available, in Fe IX/X 17.1 nm and Fe XV 28.4 nm), show a number of systematic properties that provide information about the magnetic structure of the filaments as well as about the eruption process itself:

1. The brightenings occur during the rapid ascent of the filament, as its dark, thread-like legs are pulled upward into a quasi-vertical orientation. They reach their maximum intensity when the transient coronal holes form, and subsequently fade away.
2. Multiple brightenings are usually seen, indicating that the filament has multiple endpoints that light up in succession.
3. The brightenings tend to be situated near the outer boundaries of the transient holes, and are distinct from the post-eruption arcade, whose instantaneous footpoints delineate the inner boundaries of the transient holes.
4. Comparisons with magnetograms show that the brightenings are located in and around strong unipolar network well outside the filament channel and PIL. Evidently, only in such regions is there sufficient photospheric flux to anchor the axial field of the filament.
5. The magnetic polarity of the endpoints determines the direction of the axial field component. In agreement with the empirical rule of Martin (1998), all of the dextral filaments in our sample had right-bearing barbs, while the single sinistral filament (located in the southern hemisphere) had left-bearing barbs. Furthermore, when the filament was dextral (sinistral), the post-eruption arcade had left-handed (right-handed) helicity.

We interpret the endpoint brightenings as evidence for field-line reconnection between the rapidly ascending, rotating filament and the overlying coronal arcade, as predicted (for example) in three-dimensional MHD simulations of kink-unstable filaments. This leading-edge reconnection involves the filament itself and is driven by its eruption, not the other way around. It is also distinct from the reconnection that occurs in the wake of the filament and that gives rise to the post-event arcade.

The observation of dark threads rooted far from the filament channel and PIL seems difficult to reconcile with the picture of a filament as a collection of magnetic dips supporting cool material, since such dips would not be expected to be present above strong unipolar network. On the other hand, the observation is consistent with the concept of a filament as a dynamical system of continual upflows and downflows driven by reconnection events in the chromosphere.

As noted in Section 1, the helicity implied by the filament barbs, if interpreted as concave-downward structures, is opposite to that of the overlying coronal arcade. If the rotation of the erupting filament is determined by the net helicity of the system, it would then appear that in most cases (including the events of 1997 October 23 and 2002 September 15, where dextral filaments with right-bearing barbs rotate counterclockwise) the helicity is dominated by that of the overlying arcade.

The question of whether active region filaments exhibit similar endpoint brightenings will be addressed in another study.

We are indebted to the EIT, MDI, and LASCO teams for the *SOHO* observations, and to NSO/Kitt Peak for the magnetograph data used in our potential field extrapolations. This work was supported by NASA and the Office of Naval Research.

REFERENCES

Amari, T., Luciani, J. F., Aly, J. J., Mikic, Z., & Linker, J. 2003, ApJ, 595, 1231
Amari, T., Luciani, J. F., Mikic, Z., & Linker, J. 1999, ApJ, 518, L57
Antiochos, S. K., Dahlburg, R. B., & Klimchuk, J. A. 1994, ApJ, 420, L41
Antiochos, S. K., DeVore, C. R., & Klimchuk, J. A. 1999, ApJ, 510, 485
Attrill, G., Nakwacki, M. S., Harra, L. K., van Driel-Gesztelyi, L., Mandrini, C. H., Dasso, S., & Wang, J. 2006, Sol. Phys., 238, 117
Aulanier, G., & Démoulin, P. 1998, A&A, 329, 1125
Aulanier, G., Démoulin, P., Mein, N., van Driel-Gesztelyi, L., Mein, P., & Schmieder, B. 1999, A&A, 342, 867
Brueckner, G. E., et al. 1995, Sol. Phys., 162, 357
Chae, J., Moon, Y.-J., & Park, Y.-D. 2005, ApJ, 626, 574
Delaboudinière, J.-P., et al. 1995, Sol. Phys., 162, 291
de Toma, G., Holzer, T. E., Burkepile, J. T., & Gilbert, H. R. 2005, ApJ, 621, 1109
Fan, Y. 2005, ApJ, 630, 543
Foukal, P. 1971, Sol. Phys., 19, 59
Gibson, S. E., & Fan, Y. 2006a, J. Geophys. Res., 111, A12103
Gibson, S. E., & Fan, Y. 2006b, ApJ, 637, L65
Gibson, S. E., & Fan, Y. 2008, J. Geophys. Res., 113, A09103
Green, L. M., Kliem, B., Török, T., van Driel-Gesztelyi, L., & Attrill, G. D. R. 2007, Sol. Phys., 246, 365
Kahler, S. W., & Hudson, H. S. 2001, J. Geophys. Res., 106, 29239
Kliem, B., Titov, V. S., & Török, T. 2004, A&A, 413, L23
Kopp, R. A., & Pneuman, G. W. 1976, Sol. Phys., 50, 85
Kucera, T. A., Tovar, M., & De Pontieu, B. 2003, Sol. Phys., 212, 81
Lin, Y., Engvold, O., Rouppe van der Voort, L., Wiik, J. E., & Berger, T. E. 2005, Sol. Phys., 226, 239
Lin, Y., Engvold, O., & Wiik, J. E. 2003, Sol. Phys., 216, 109
Lites, B. W. 2005, ApJ, 622, 1275
Litvinenko, Y. E., & Martin, S. F. 1999, Sol. Phys., 190, 45
Liu, Y., & Hayashi, K. 2006, ApJ, 640, 1135
López Ariste, A., Aulanier, G., Schmieder, B., & Sainz Dalda, A. 2006, A&A, 456, 725
Low, B. C. 1996, Sol. Phys., 167, 217
Mackay, D. H., Gaizauskas, V., & van Ballegooijen, A. A. 2000, ApJ, 544, 1122
Manchester, W., IV, Gombosi, T., DeZeeuw, D., & Fan, Y. 2004, ApJ, 610, 588
Martin, S. F. 1998, Sol. Phys., 182, 107
Martin, S. F. 2003, Adv. Space Res., 32, 1883
Martin, S. F., Lin, Y., & Engvold, O. 2008a, Sol. Phys., 250, 31
Martin, S. F., & McAllister, A. H. 1997, in Coronal Mass Ejections, ed. N. Crooker, J. A. Joselyn, & J. Feynman (Geophys. Monogr. 99; Washington, DC: AGU), 127
Martin, S. F., Panasenco, O., Engvold, O., & Lin, Y. 2008b, Ann. Geophys., 26, 3061
McIntosh, S. W., Leamon, R. J., Davey, A. R., & Wills-Davey, M. J. 2007, ApJ, 660, 1653
Metcalf, T. R., et al. 2006, Sol. Phys., 237, 267
Moore, R. L., Sterling, A. C., Hudson, H. S., & Lemen, J. R. 2001, ApJ, 552, 833
Okamoto, T. J., et al. 2008, ApJ, 673, L215
Pevtsov, A. A., Balasubramaniam, K. S., & Rogers, J. W. 2003, ApJ, 595, 500
Reinard, A. A., & Biesecker, D. A. 2008, ApJ, 674, 576
Roussev, I. I., Forbes, T. G., Gombosi, T. I., Sokolov, I. V., DeZeeuw, D. L., & Birn, J. 2003, ApJ, 588, L45
Rust, D. M., & Kumar, A. 1994, Sol. Phys., 155, 69
Rust, D. M., & LaBonte, B. J. 2005, ApJ, 622, L69
Scherrer, P. H., et al. 1995, Sol. Phys., 162, 129
Sterling, A. C., & Moore, R. L. 2004, ApJ, 602, 1024
Sterling, A. C., & Moore, R. L. 2005, ApJ, 630, 1148
Titov, V. S., & Démoulin, P. 1999, A&A, 351, 707
Török, T., & Kliem, B. 2005, ApJ, 630, L97
van Ballegooijen, A. A., & Martens, P. C. H. 1989, ApJ, 343, 971
Wang, Y.-M. 1999, ApJ, 520, L71
Wang, Y.-M. 2001, ApJ, 560, 456
Wang, Y.-M., & Muglach, K. 2007, ApJ, 666, 1284
Yeates, A. R., & Mackay, D. H. 2009, Sol. Phys., 254, 77
Yeates, A. R., Mackay, D. H., & van Ballegooijen, A. A. 2007, Sol. Phys., 245, 87
Zirker, J. B., Engvold, O., & Martin, S. F. 1998, Nature, 396, 440
Zirker, J. B., Martin, S. F., Harvey, K., & Gaizauskas, V. 1997, Sol. Phys., 175, 27